

Constellation Selection and Power Control for OFDM-based ISAC: From Theory to Prototype

Kaitao Meng, *Member, IEEE*, Kawon Han, *Member, IEEE*, Christos Masouros, *Fellow, IEEE*, and Fan Liu, *Senior Member, IEEE*

Abstract—Integrated sensing and communication (ISAC) techniques can leverage existing, wide-coverage communication networks to perform sensing tasks, enabling large-scale and low-cost target sensing. However, the inherent randomness of communication data payloads introduces undesired sidelobes in the ambiguity function that may degrade target detection and parameter estimation performance. This paper develops a communication-centric ISAC framework that is standards-compliant and compatible with existing devices. Specifically, we propose a low-complexity constellation selection scheme over a *finite, off-the-shelf* alphabet, achieving an efficient sensing-communication trade-off without custom waveforms or frame-structure changes. To this end, we analyze two classical sensing receivers including matched filtering (MF) and reciprocal filtering (RF) for ranging measurements, and derive closed-form sensing laws that link constellation statistics to sensing performance. Under any finite-alphabet constellation combination, MF sidelobes depend on the weighted sum of the kurtosis values of the per-subcarrier constellations, while RF noise enhancement depends on the inverse second moment of the transmit symbol, providing a tractable expression for tuning the sensing-communication trade-off. The analysis extends to multi-symbol coherent integration and achieves the expected processing gain. Guided by these insights, we propose a low-complexity design that retains a finite constellation set and optimally shapes power under communication quality constraints. We prove that in flat-fading channels, any Pareto-optimal solution activates no more than three constellations. For frequency-selective channels, a bilevel algorithm with closed-form inner updates attains near-optimal performance while sharply reducing computational complexity. We validate the entire theoretical pipeline with numerical simulations as well as experimental results. The results corroborate the theory, constellation mixing and coherent multi-symbol processing reliably reveal markedly weaker targets at practical signal-to-noise ratios.

Index Terms—Integrated sensing and communication (ISAC), constellation design, ambiguity function sidelobes, matched filtering, reciprocal filtering, adaptive modulation, kurtosis, coherent integration, SDR experiments.

I. INTRODUCTION

High-precision localization and high-rate data delivery underpin emerging applications such as autonomous driving and advanced augmented reality [1], [2]. Operating separate sensing and communication (S&C) stacks duplicates front-end hardware and frame structures, leads to uncoordinated spectrum

use and mutual interference, motivating integrated sensing and communication (ISAC) techniques [3]–[7]. By reusing infrastructure, spectrum, and configurable waveforms, ISAC enables simultaneous data transmission and echo-based perception with quantifiable gains in spectral, energy, and cost efficiency [8], [9]. The unified architecture further permits joint design of waveform [10], novel frame structure [11], and resource allocation to balance rate, reliability, and sensing resolution under common constraints [12], [13]. Beyond link-level co-design, recent work elevates ISAC to the network-level cooperation for interference control [14], cooperative sensing [15], and cross-link scheduling [16]. Consistent with this trajectory, ISAC has been identified by the ITU as a representative 6G usage scenario.

Given the ubiquity of cellular infrastructure already providing wide-area coverage, communication-centric ISAC designs that reuse existing waveforms and frame structures are attractive for near-term deployment because they adhere to existing standards and remain compatible with legacy devices [17], [18]. A practical obstacle, however, is that data payload symbols are inherently random [19], this randomness translates into ambiguity-function sidelobe variability that can mask weak targets or create ghost peaks [20]. Therefore, understanding how the modulation constellation shapes the sensing-communication trade-off is thus essential. Constellation design operates at the modulation layer, where optimizing the symbol alphabet shapes the statistics that set ambiguity-function sidelobes and effective noise. Although constellation optimization offers a lightweight lever, realizing it in an implementable, standards-aligned manner is non-trivial and remains an open problem [21]. This motivates deeper investigation of standards-compliant constellation shaping, mixing, and selection strategies that preserve the waveform, alphabet/bit-mapping, and 5G new radio (NR) time-frequency resource grid.

Recent work has sharpened the link between data-modulation (constellation mapping) and sensing performance. In particular under single antenna transmission, [22] establishes the ranging optimality of OFDM, and multiple studies show that PSK constellations often yield lower range-sidelobe levels than QAM, thereby improving delay resolution and ambiguity suppression [23], [24]. Moreover, ambiguity-function variance is governed by constellation kurtosis, so high-kurtosis signaling leads to larger sidelobe fluctuations [25]. Complementary to these results, [26] analyzes sensing performance under a uniform signaling setup, where all subcarriers use the same constellation with fixed power, and proves that OFDM is optimal for ranging. In parallel, early studies pursue constellation optimization approaches to modify the signal alphabet itself to

K. Meng is with the Department of Electrical and Electronic Engineering, University of Manchester, Manchester, UK (email: kaitao.meng@manchester.ac.uk). K. Han is with the Department of Electrical Engineering, Ulsan National Institute of Science and Technology (UNIST), Ulsan, South Korea (emails: kawon.han@unist.ac.kr). C. Masouros is with the Department of Electronic and Electrical Engineering, University College London, London, UK (email: c.masouros@ucl.ac.uk). F. Liu is with the National Mobile Communications Research Laboratory, Southeast University, China (emails: fan.liu@seu.edu.cn).

target theoretical performance limits [27]–[30]. However, such redesigns are difficult to deploy in practical systems because they depart from standardized constellations, forcing receiver demapper and invalidating existing link-adaptation tables. These limitations motivate a standards-compliant alternative: Retain the existing constellation set, select suitable members per scenario, and jointly shape power to satisfy communication QoS while improving sensing. To our knowledge, a low-complexity method that performs this adaptive constellation selection and subcarrier power control has been largely underexplored.

To address the above gap, in this paper we propose a low-complexity, standards-compliant scheme for adaptive constellation selection and subcarrier power control. Unlike conventional communication power control, which targets rate or QoS alone [31], our design introduces an explicit degree of freedom to balance sensing and communication via joint power and constellation control. Specifically, we model the payload explicitly as a random process and develop an OFDM-based, communication-centric ISAC co-design that is compatible with existing standards. We analyze two canonical sensing receiver chains: matched filtering (MF) [32] and reciprocal filtering (RF) [33]. RF suppresses target/clutter sidelobes by equalizing data dependence but incurs a waveform-dependent SNR loss relative to MF, yielding a tunable trade-off. While [34] contrasts MF and RF sidelobes as a function of target SNR, a rigorous, end-to-end characterization of how per-subcarrier constellation design and power allocation propagate through MF/RF chains to determine OFDM sensing performance (e.g., range-sidelobe levels, estimation accuracy) remains largely open. To address this issue, we derive closed-form performance laws that expose the roles of constellation moments: (i) MF sidelobe power is dictated by the per-subcarrier fourth moment; (ii) RF noise amplification is governed by the inverse second moment of modulated signals. The analysis extends to multi-symbol coherent integration and yields the expected gain, which we exploit for super-resolution delay estimation via a Matrix Pencil estimator. Rather than redesigning alphabets, we select from a finite, standards-compliant constellation pool and shape power. This is compatible with existing OFDM protocols and demappers. The main contributions of this paper are summarized as follows:

- We propose a low-complexity, standards-compliant scheme for adaptive constellation selection and subcarrier power control in ISAC systems, by mixing a small set of off-the-shelf constellations across subcarriers and optimally allocates power under communication quality constraints. We derive closed-form sensing laws that decouple constellation statistics from power allocation. For MF, sidelobes are governed by the sum of constellation fourth moment of subcarriers; for RF, the effective noise is governed by the sum of the inverse second moment of the transmitted symbols. The analysis extends to multi-symbol coherent integration and predicts a processing gain that increases with the number of integrated symbols, reducing ambiguity-function sidelobes and effective noise variance.
- The above laws imply two sensing-optimal power-allocation rules: With MF, allocate less power to subcarriers whose constellations have higher kurtosis; with RF, allocate

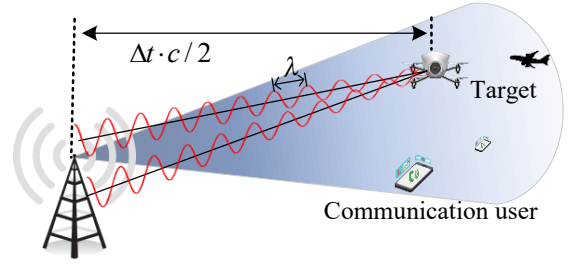


Fig. 1. Scenarios of ranging measurements using same communication signals.

more power to subcarriers with larger inverse second moment. Moreover, within any subset of subcarriers sharing the same constellation statistics, equal power is provably optimal, which can facilitate power allocation efficiency.

- In flat fading channels, any optimal operating point for the considered constellation selection problem activates at most three constellations, collapsing the search from a high-dimensional simplex to a finite set of low-cardinality mixtures. Compared with fixed-power analyses in which all subcarriers use a single constellation, our method delivers a provably optimal, standards-compliant heterogeneous mixture policy. For frequency-selective channels we design a bilevel scheme that maintains binary constellation decisions at every iterate. The method attains near-optimal performance at a fraction of the complexity.
- Experiments corroborate the theory: Lower sidelobes as the constant-envelope share increases, achieving detection of targets up to roughly ten decibels weaker, which is consistent with coherent gain consistent with analysis. It also verifies that MF is preferable at low SNR, while RF dominates at high SNR when MF becomes sidelobe-limited.

Section II presents the system, signal, and detection models (MF/RF) and defines ESL. Section III derives single- and multi-symbol sensing expressions and RF noise analysis. Section IV develops optimal power rules and the joint constellation and power formulations, including structural results and scalable algorithms. Section V reports simulations and Pluto-SDR experiments. Section VI concludes.

II. SYSTEM MODEL

We consider a monostatic ISAC system employing an OFDM waveform, and propose a low-complexity constellation design to reveal a new trade-off between sensing and communication, while maintaining compatibility with existing communication standards. The ISAC transmitter emits signals modulated with random communication symbols, which are received by several communication users and simultaneously reflected back to the sensing receiver by Q targets at different ranges, as shown in Fig. 1. The sensing receiver employs classical signal processing techniques such as MF and RF to estimate the range of targets using the known transmitted signals.

A. Signal Model

Let $\mathbf{s} = [s_0, s_1, \dots, s_{N-1}]^T \in \mathbb{C}^{N \times 1}$ denote the transmitted symbol vector over N subcarriers, where each s_n is indepen-

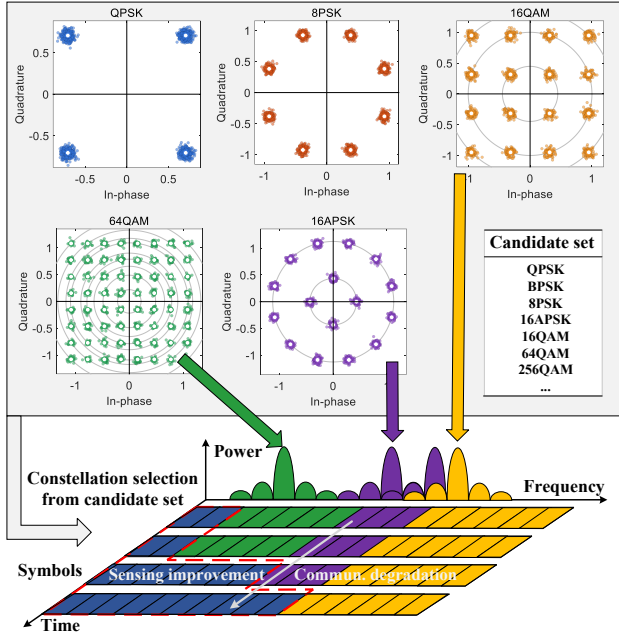


Fig. 2. Illustration of constellation selection to balance sensing and communication performance.

dently drawn from a complex constellation set $\mathcal{C} = \{c_1, \dots, c_J\}$ (i.e., the set of available modulation constellations (e.g., QPSK, QAM, APSK)) based on the requirements of sensing and communication performance, as shown in Fig. 2, where J denotes the number of candidate constellations. We assume zero-mean, unit-power symbols, i.e., $\mathbb{E}(s_n) = 0$ and $\mathbb{E}(|s_n|^2) = 1$. The kurtosis of the constellation on subcarrier n is defined as [35]

$$\mu_{4,n} \triangleq \frac{\mathbb{E}\{|s_n - \mathbb{E}(s_n)|^4\}}{\mathbb{E}\{|s_n - \mathbb{E}(s_n)|^2\}^2}, \quad (1)$$

with $\mu_{4,n} \geq 1$. The expected inverse second moment on subcarrier n [34] is defined as

$$\nu_{-2,n} = \mathbb{E}[|s_n|^{-2}]. \quad (2)$$

We adopt the unitary N -point DFT/IDFT for OFDM modulation. The corresponding time-domain OFDM signal is generated by an N -point inverse discrete Fourier transform (IDFT), the discrete-time domain signal is given by

$$\mathbf{x} = \mathbf{F}_N^H \mathbf{P} \mathbf{s}, \quad (3)$$

where \mathbf{F}_N^H is the unitary IDFT matrix of size N , $\mathbf{P} = \text{diag}([\sqrt{P_0}, \dots, \sqrt{P_{N-1}}])$ denotes the power allocation matrix, and P_n represents the power allocated to the n -th subcarrier. Here, $\mathbf{x} = [x[0], \dots, x[N-1]]$, where

$$x[t] = \frac{1}{\sqrt{N}} \sum_{n=0}^{N-1} \sqrt{P_n} s_n e^{j \frac{2\pi}{N} tn}, \quad t = 0, 1, \dots, N-1. \quad (4)$$

A cyclic prefix (CP) of appropriate length is appended to mitigate inter-symbol interference, and is discarded at the receiver [36]. Assuming Q point targets with round-trip propagation delays $\{\tau_q\}_{q=1}^Q$, the received baseband signal $\mathbf{y} \in \mathbb{C}^N$ can be modeled as

$$\mathbf{y} = \sum_{q=1}^Q \alpha_q \mathbf{J}_{\tau_q} \mathbf{x} + \mathbf{z}, \quad (5)$$

where $\alpha_q \in \mathbb{C}$ is the complex reflection coefficient (including pathloss) of the q -th target, and it is assumed that $\alpha_q \in \mathbb{C} \sim \mathcal{CN}(\mathbf{0}, \sigma_{\alpha_q}^2)$. Also, $\mathbf{z} \sim \mathcal{CN}(\mathbf{0}, \sigma_z^2 \mathbf{I})$ is additive white Gaussian noise, and \mathbf{J}_k is the $N \times N$ cyclic shift matrix corresponding to delay k defined as

$$\mathbf{J}_k = \begin{bmatrix} \mathbf{0}_{(N-k) \times k} & \mathbf{I}_{N-k} \\ \mathbf{I}_k & \mathbf{0}_{k \times (N-k)} \end{bmatrix}, \quad k = 0, 1, \dots, N-1. \quad (6)$$

The delay τ_q relates to physical range d_q by $\tau_q = \lfloor \frac{2d_q}{cT_s} \rfloor$, where c is the speed of light and T_s is the sampling interval. This discrete delay simplifies the time-domain representation as cyclic shifts.

Let $X[n]$ and $Y[n]$ be the N -point DFTs of \mathbf{x} and \mathbf{y} , respectively, where $X[n] = \sqrt{P_n} s_n$. In a multi-target environment with additive white Gaussian noise (AWGN), the received frequency-domain signal can be expressed as

$$Y[n] = \sum_{q=1}^Q \alpha_q X[n] e^{-j \frac{2\pi}{N} n \tau_q} + Z[n], \quad (7)$$

B. Ranging Estimation

1) *Matched Filtering*: The receiver performs MF by correlating the received signal \mathbf{y} with the transmitted OFDM symbol \mathbf{x} . The MF output at delay (time index) t is

$$\tilde{y}^{\text{MF}}[t] = \mathbf{x}^H \mathbf{y}_t, \quad (8)$$

where $\mathbf{y}_t = [y[t], y[t+1], \dots, y[t+N-1]]^T$ is the received vector segment starting at sample t , with indices modulo N . Substituting \mathbf{y} , we obtain

$$\tilde{y}^{\text{MF}}[t] = \sum_{q=1}^Q \alpha_q \mathbf{x}^H \mathbf{J}_{\tau_q - t} \mathbf{x} + \tilde{z}^{\text{MF}}[t], \quad (9)$$

where $\tilde{z}^{\text{MF}}[t] = \mathbf{x}^H \mathbf{J}_{N-t} \mathbf{z}$, which is distributionally equivalent to $\mathbf{x}^H \mathbf{z}$ because $\mathbf{z} \sim \mathcal{CN}(\mathbf{0}, \sigma_z^2 \mathbf{I})$ and \mathbf{J}_{N-t} is unitary. The key term

$$r_k = \mathbf{x}^H \mathbf{J}_k \mathbf{x} = r_{N-k}^*, \quad k = 0, 1, \dots, N-1, \quad (10)$$

defines the periodic autocorrelation functions (ACFs) of the transmit signal \mathbf{x} . Hence, the MF output can be written as a superposition of shifted autocorrelation functions:

$$\tilde{y}^{\text{MF}}[t] = \sum_{q=1}^Q \alpha_q r_{\tau_q - t} + \tilde{z}^{\text{MF}}[t]. \quad (11)$$

MF can also be efficiently realized in the frequency domain by leveraging the convolution theorem. Specifically, the MF output in frequency domain is

$$\tilde{Y}^{\text{MF}}[n] = \sqrt{N} Y[n] X[n]^*, \quad n = 0, 1, \dots, N-1. \quad (12)$$

The time-domain MF output is recovered via IDFT as follows:

$$\tilde{y}^{\text{MF}}[t] = \frac{1}{\sqrt{N}} \sum_{n=0}^{N-1} \tilde{Y}^{\text{MF}}[n] e^{j \frac{2\pi}{N} nt}. \quad (13)$$

Without loss of generality, let $q \in \mathcal{Q}$ denote the target of interest, and echoes from all $k \in \mathcal{Q} \setminus \{q\}$ are modeled as clutter. To quantify the sensing quality under multi-target scenarios and additive noise, we define an effective signal-to-interference-plus-noise ratio (SINR) to reveal the relationship between the signal after receive signal processing and sensing

task performance. Specifically, the effective SINR at the true delay τ_q of the q -th target can be defined by

$$\text{SINR}_q = \frac{\mathbb{E} \left[|s_q[\tau_q]|^2 \right]}{\mathbb{E} \left[|\tilde{y}[\tau_q] - s_q[\tau_q]|^2 \right]}, \quad (14)$$

where $\tilde{y}[t]$ is the total output of the sensing filter at delay t , and $s_q[t]$ denotes the desired signal contribution from the q -th target, i.e., the noise-free component at that location. Then, $\tilde{y}[t]$ is a superposition of delayed ACFs plus filtered noise, given by $\tilde{y}[t] = \sum_{q=1}^Q \alpha_q r_{\tau_q-t} + \tilde{z}[t]$. The desired signal term is $s_q[t] = \alpha_q r_{\tau_q-t}$, while the remaining part of $\tilde{y}[t]$ corresponds to clutter interference from the other targets and filtered noise. Thus

$$\text{SINR}_q^{\text{MF}} = \frac{|\alpha_q|^2 \mathbb{E}[|r_0|^2]}{\sum_{p \neq q} |\alpha_p|^2 \mathbb{E}[|r_{\tau_q - \tau_p}|^2] + \mathbb{E}[|\tilde{z}[\tau_q]|^2]}. \quad (15)$$

Remark 1: In (15), $\mathbb{E}[|r_0|^2]$ captures the mainlobe energy at the true delay, and $\mathbb{E}[|r_{\tau_q - \tau_p}|^2]$ are the sidelobe levels at the relative delays of other targets (masking terms). Therefore, (15) is exactly a peak-to-sidelobe-plus-noise ratio that governs the probability that $|\tilde{y}^{\text{MF}}[\tau_q]|^2$ exceeds a detection threshold. In the single-target case ($Q = 1$) it reduces to the standard MF SNR.

2) *Reciprocal Filtering:* RF operates entirely in the frequency domain [33]. Given the N -point DFTs of the transmitted and received signals, denoted by $X[n]$ and $Y[n]$, respectively, RF performs element-wise division as follows:¹

$$\hat{Y}^{\text{RF}}[n] = Y[n]/X[n], \quad n = 0, \dots, N-1. \quad (16)$$

The time-domain output is then obtained by inverse DFT, i.e.,

$$\tilde{y}^{\text{RF}}[t] = \frac{1}{\sqrt{N}} \sum_{n=0}^{N-1} \hat{Y}^{\text{RF}}[n] e^{j \frac{2\pi}{N} nt}. \quad (17)$$

Substituting (7) into the RF procedure (16) yields

$$\tilde{y}^{\text{RF}}[t] = \sum_{q=1}^Q \alpha_q \underbrace{\frac{1}{\sqrt{N}} \sum_{n=0}^{N-1} e^{j \frac{2\pi}{N} n(t - \tau_q)}}_{\mathcal{D}_N(t - \tau_q)} + \tilde{z}^{\text{RF}}[t], \quad (18)$$

where $\mathcal{D}_N(\cdot)$ is the periodic Dirichlet kernel, and it reduces to an ideal discrete impulse when τ_q is an integer (mod N), otherwise exhibits a sinc-function (or sinc-like function) pattern, i.e., spectral leakage. In (18), $\tilde{z}^{\text{RF}}[t]$ is the filtered noise shaped by $\frac{Z[n]}{X[n]}$. Then, the RF-based signal-to-noise ratio (SNR) can be written as

$$\text{SNR}_q^{\text{RF}} = \frac{|\alpha_q|^2 |\mathcal{D}_N|^2}{\mathbb{E}[|\tilde{z}^{\text{RF}}[\tau_q]|^2]}, \quad (19)$$

where $|\mathcal{D}_N| = \sqrt{N}$. It can be observed that unlike the SINR expression for MF, $\tilde{y}^{\text{RF}}[t]$ does not include sidelobe interference terms in the denominator. This is because RF performs a symbol-wise division by the known communication symbols, effectively equalizing the frequency-domain response of each subcarrier. However, the symbol-wise division inherent in RF alters the noise statistics, which can increase the effective noise variance. Specifically, in (18), $\tilde{z}^{\text{RF}}[t]$ is the spectrally shaped noise introduced by dividing $Y[n]$ by $X[n]$ in the frequency

¹We assume $s_n \neq 0$ almost surely and implement reciprocal filtering via a Tikhonov-regularized division to avoid blow-ups when $|X[n]|$ is small: $\hat{Y}^{\text{RF}}[n] = \frac{Y[n] X[n]^*}{|X[n]|^2 + \varepsilon}$, $\varepsilon > 0$.

domain.

3) *Matrix Pencil Delay Estimation:* To capture sub-sample (fractional) delays, we adopt an equivalent continuous-phase parametric model. Conventional delay estimation based on peak picking in $\tilde{y}^{\text{MF}}[n]$ or $\tilde{y}^{\text{RF}}[n]$ is limited by the sampling grid, whereas the Matrix Pencil (MP) method [37] enables super-resolution by exploiting the phase progression of complex exponentials embedded in structured data matrices. Based on the discussion in II-B, let $e[n] = \hat{Y}^{\text{MF}}[n]$ and $e[n] = \hat{Y}^{\text{RF}}[n]$. Build Hankel matrices of size $L \times K$ with $L = N - K$ and $K \approx N/2$:

$$E_1 = \begin{bmatrix} e[0] & e[1] & \cdots & e[K-1] \\ e[1] & e[2] & \cdots & e[K] \\ \vdots & \vdots & \ddots & \vdots \\ e[L-1] & e[L] & \cdots & e[L+K-2] \end{bmatrix}, \quad (20)$$

$$E_2 = \begin{bmatrix} e[1] & e[2] & \cdots & e[K] \\ e[2] & e[3] & \cdots & e[K+1] \\ \vdots & \vdots & \ddots & \vdots \\ e[L] & e[L+1] & \cdots & e[L+K-1] \end{bmatrix}. \quad (21)$$

Choose $Q < \min\{K, L\}$ and compute the rank- Q truncated SVD $E_1 \approx U \Sigma V^H$ with $U \in \mathbb{C}^{L \times Q}$, $\Sigma \in \mathbb{R}^{Q \times Q}$, $V \in \mathbb{C}^{K \times Q}$. Solve

$$\Sigma^{-1} U^H E_2 V \mathbf{v}_q = \lambda_q \mathbf{v}_q, \quad (22)$$

which ideally yields $\lambda_q = e^{-j \frac{2\pi}{N} \tau_q}$. The delays are then

$$\hat{\tau}_q = -\frac{N}{2\pi} \arg(\lambda_q) \bmod N, \quad q = 1, \dots, Q. \quad (23)$$

C. Communication Model and Performance Metrics

Following communication standards, the system supports downlink communication by embedding information within the frequency-domain symbols s_n . For practical engineering considerations, the system employs a fixed, known discrete constellation set \mathcal{C} for modulation. Let $\mathcal{C}_j \subset \mathbb{C}$ denote the constellation set of mode j , and let $|\mathcal{C}_j|$ be its size. The uncoded bits per symbol is $\log_2 |\mathcal{C}_j|$ bits/symbol. Let $\chi_{n,j} \in \{0, 1\}$ indicate that subcarrier n uses constellation $j \in \{1, \dots, J\}$. Then, the aggregate number of raw bits per OFDM symbol across all users is given by:

$$R_{\text{com}} = \sum_{n=0}^{N-1} \sum_{j=1}^J \chi_{n,j} \log_2 |\mathcal{C}_j|. \quad (24)$$

To ensure reliable transmission, the bit error rate (BER) on each subcarrier must remain below a predefined threshold, i.e., if the SNR

$$\sum_{j=1}^J \chi_{n,j} \text{BER}_j(\gamma_n) \leq \text{BER}_{\text{th}}, \quad \forall n, \quad (25)$$

where $\gamma_n = \frac{|H_n|^2 P_n}{N_0 \Delta f}$, and H_n is the complex channel gain on subcarrier n . We denote N_0 as the single-sided noise power spectral density, and Δf as subcarrier spacing. Under AWGN with coherent detection and Gray mapping, BER admits closed forms, e.g., for QPSK $\text{BER}_{\text{QPSK}}(\gamma) = Q(\sqrt{\gamma})$ and for square

M -QAM $\text{BER}_{\text{QAM}}(\gamma) \approx \frac{4}{\log_2 M} \left(1 - \frac{1}{\sqrt{M}}\right) Q(\sqrt{3\gamma/(M-1)})$, where γ is the per-subcarrier symbol SNR. Alternatively, we tabulate BER-SNR curves per constellation (including APSK and coded MCS) and apply monotone interpolation/inversion to obtain γ_j^{\min} and thus $P_{n,j}^{\min}$ for a given BER target.

D. Problem Formulation

Communication-centric ISAC entails a communication performance guarantee while maximising sensing performance. Since the optimization ultimately targets sidelobe suppression rather than the performance of any specific target, the formulation does not depend on individual target characteristics. We jointly optimize constellation selection and power allocation over N subcarriers to maximize sensing performance while guaranteeing communication requirements:

$$(P1) \quad \max_{\mathbf{x}, \mathbf{P}} \quad \text{SINR}_s(\mathbf{x}, \mathbf{P}) \quad (26a)$$

$$\text{s.t.} \quad \frac{1}{N} R_{\text{com}} \geq R_{\min}, \quad (26b)$$

$$\sum_{j=1}^J \chi_{n,j} \text{BER}_j(\gamma_n) \leq \text{BER}_{\text{th}}, \forall n, \quad (26c)$$

$$\frac{1}{N} \sum_{n=0}^{N-1} P_n = P_{\text{ave}}, P_n \geq 0, \forall n, \quad (26d)$$

$$\sum_{j=1}^J \chi_{n,j} = 1, \chi_{n,j} \in \{0, 1\}, \forall n, j. \quad (26e)$$

where $\text{SINR}_s(\mathbf{x}, \mathbf{P}) \in \{\text{SINR}_q^{\text{MF}}, \text{SNR}_q^{\text{RF}}\}$ denotes the output SINR after sensing receive filtering. Here, (26b) and (26c) respectively represent communication spectral efficiency constraint and communication BER constraint. (26d) ensures the total power constraint of all subcarriers. The resulting mixed-integer nonlinear programming (MINLP) problem explicitly captures the sensing-communication tradeoff, as the choice of constellation and power on each subcarrier jointly affects both the communication rate and the sensing SINR of MF (SNR of RF) through the fourth-order moment $\mu_{4,n}$ (the inverse second moment $\nu_{-2,n}$) and the BER expression.

III. ANALYTICAL STUDY OF THE SENSING PERFORMANCE

In this section, we systematically investigate the closed-form expressions of sensing SINR output as a function of the employed constellation and the allocated power, in the considered ISAC system.

A. SINR Expression for Matched Filtering

Since \mathbf{x} depends on the random transmitted symbols $\{s_n\}$, r_k is a random process. The average system performance of MF is thus highly determined via the expected autocorrelation power $\mathbb{E}[|r_k|^2]$, which provides insight into average sidelobe levels and range resolution [26]. In (15), the relative delays $\Delta_{qi} \triangleq (\tau_q - \tau_i) \bmod N$ are unknown and can be modeled as random, approximately uniform over $\{1, \dots, N-1\}$. Hence, the expected autocorrelation power over nonzero delays is

$$\mathbb{E}_{\Delta} \left[\mathbb{E}[|r_{\Delta}|^2] \right] = \frac{1}{N-1} \sum_{k=1}^{N-1} \mathbb{E}[|r_k|^2]. \quad (27)$$

To this end, the expected clutter interference caused by sidelobe of ACFs can be given by $I_q \approx (\sum_{i \neq q} |\alpha_i|^2)$ ESL. Then, we define an important component, the *expected sidelobe level* (ESL), given by

$$\text{ESL} = \frac{1}{N-1} \sum_{k=1}^{N-1} \mathbb{E}[|r_k|^2]. \quad (28)$$

Physically, the ESL can be interpreted as the level of matched-filter output interference at the target location caused by other interfering scatterers in the presence of clutter. We next analyze the sensing performance expressions for both single-symbol and multi-symbol cases, highlighting the coherent integration gain achievable in each scenario.

1) *Single OFDM Symbol*: We first analyze the sensing SINR for the case of a single OFDM symbol. For the zero-lag term $k=0$, we have $r_0 = \sum_{n=0}^{N-1} P_n |s_n|^2$, denoting the peak of the auto-correlation results. Using independence across subcarriers and $\mathbb{E}[|s_n|^2] = 1$, it follows that

$$\begin{aligned} \mathbb{E}[|r_0|^2] &= \sum_{n=0}^{N-1} P_n^2 \mathbb{E}[|s_n|^4] + \sum_{\substack{n, n'=0 \\ n \neq n'}}^{N-1} P_n P_{n'} \mathbb{E}[|s_n|^2] \mathbb{E}[|s_{n'}|^2] \\ &= \sum_{n=0}^{N-1} P_n^2 (\mu_{4,n} - 1) + \left(\sum_{n=0}^{N-1} P_n \right)^2. \end{aligned} \quad (29)$$

In (29), under equal (or not-too-peaky) power allocation, the relative contribution of the first term is very small for large N . In particular, for constant-modulus constellations (e.g., PSK) where $\mu_{4,n} = 1$, the first term vanishes exactly. Therefore, we simplify $\mathbb{E}[|r_0|^2]$ as $\left(\sum_{n=0}^{N-1} P_n \right)^2$ in the following optimization design.

Proposition 1: The expected sidelobe level can be given by

$$\text{ESL} = \frac{1}{N-1} \left(\sum_{n=0}^{N-1} [(N-1)\mu_{4,n} + 1] P_n^2 - \left(\sum_{n=0}^{N-1} P_n \right)^2 \right). \quad (30)$$

Proof: Please refer to Appendix A. ■

Based on Proposition 1, the SINR of sensing receiver signal after receive filtering can be given by

$$\text{SINR}_q^{\text{MF}} = \frac{|\alpha_q|^2 \mathbb{E}[|r_0|^2]}{\sum_{i \neq q} |\alpha_i|^2 \text{ESL} + \sigma_z^2 \sum_{n=0}^{N-1} P_n}. \quad (31)$$

Based on (31), the SINR is maximized when the kurtosis equals 1. Therefore, to enhance performance, one should select as many subcarriers as possible with kurtosis equal to 1, such as those modulated using constant-modulus schemes like QPSK. As evident from (30), the ESL is invariant to any permutation of the subcarrier constellation order, enabling us to exploit this property for sensing and communication optimization. Importantly, the reflection coefficient $|\alpha_q|^2$ can be approximated by its expected value $\mathbb{E}[|\alpha_q|^2] = \sigma_{\alpha_q}^2$ to facilitate the analysis, as this parameter can be ignored when maximizing $\text{SINR}_s(\mathbf{x}, \mathbf{P})$.

2) *Multi-Symbol Coherent Processing Gain*: We consider an OFDM system with N subcarriers and sense over M independent OFDM symbols to enhance coherent processing gain. This is achieved by accumulating multiple OFDM symbols under the assumption that the target remains approximately stationary within a short time interval. The m -th transmitted

OFDM symbol in the time domain is given by

$$x^{(m)}[t] = \frac{1}{\sqrt{N}} \sum_{n=0}^{N-1} \sqrt{P_n} s_n^{(m)} e^{j\frac{2\pi}{N}nt}, \quad t = 0, \dots, N-1,$$

where the data symbols $s_n^{(m)}$ are i.i.d. with $\mathbb{E}[|s_n^{(m)}|^2] = 1$ and kurtosis $\mathbb{E}[|s_n^{(m)}|^4] = \mu_{4,n}$.

The averaged ACF at lag k over M symbols is defined as

$$\bar{r}_k = \frac{1}{M} \sum_{m=1}^M r_k^m = \frac{1}{M} \sum_{m=1}^M \sum_{n=0}^{N-1} P_n |s_n^{(m)}|^2 e^{j\frac{2\pi}{N}nk}, \quad (32)$$

where r_k^m denotes the ACF of the m th realization.

Theorem 1: For coherent processing of M independent OFDM symbols, the SINR at the MF output for the q -th target is

$$\text{SINR}_q^{\text{MF}} = \frac{\sigma_{\alpha_q}^2 \mathbb{E}[|\bar{r}_0|^2]}{\frac{\sum_{i \neq q} \sigma_{\alpha_i}^2}{N-1} \sum_{k=1}^{N-1} \mathbb{E}[|\bar{r}_k|^2] + \frac{\sigma_z^2}{M} \sum_{n=0}^{N-1} P_n}, \quad (34)$$

where $\mathbb{E}[|\bar{r}_0|^2] = \frac{1}{M} \sum_{n=0}^{N-1} P_n^2 (\mu_{4,n} - 1) + \left(\sum_{n=0}^{N-1} P_n \right)^2$, and $\sum_{k=1}^{N-1} \mathbb{E}[|\bar{r}_k|^2] = \frac{N-1}{M} \sum_{n=0}^{N-1} P_n^2 (\mu_{4,n} - 1) + N \sum_{n=0}^{N-1} P_n^2 - \left(\sum_{n=0}^{N-1} P_n \right)^2$.

Proof: Please refer to Appendix B. ■

These expressions explicitly demonstrate how coherent processing (increasing M) reduces random sidelobes and noise effects, leaving structural sidelobes unchanged, thus guiding effective waveform optimization.

B. SNR Analysis for Reciprocal Filtering

To quantify the performance of reciprocal filtering, we derive its theoretical SNR by analyzing the noise statistics after symbol-wise division in the frequency domain.

Theorem 2: For coherent processing over M independent OFDM symbols, the theoretical SNR for reciprocal filtering is

$$\text{SNR}_q^{\text{RF}} = \frac{\sigma_{\alpha_q}^2 M N^2}{\sigma_z^2 \sum_{n=0}^{N-1} \frac{\nu_{-2,n}}{P_n}}. \quad (35)$$

Proof: Please refer to Appendix C. ■

From the above analysis, it is evident that increasing the number of coherently processed symbols leads to a monotonic improvement in effective SNR. This enhancement significantly improves ranging accuracy when detecting quasi-static targets. However, for non-static targets, the number of coherent symbols should be carefully selected based on the target's velocity to avoid additional interference caused by target movement.

IV. PROPOSED ALGORITHM DESIGN AND PERFORMANCE ANALYSIS

A. Sensing-Optimal performance

When communication performance requirements are disregarded, the problem reduces to maximizing sensing performance alone. It is straightforward to observe that when the modulation constellation satisfies $\mu_{4,n} = 1$ and $\nu_{-2,n} = 1$, both interference term of MF and noise term of RF are minimized. In the general case, where the constellation does not have these ideal properties, the optimal power allocation can be analyzed as follows.

Based on the analysis in Section III-A1, we can simplify the expression of SINR of MF results, and thus minimize the ESL instead of maximizing SINR, i.e., $\text{SINR}_q^{\text{MF}} \approx \frac{\sigma_{\alpha_q}^2 N^2 P_{\text{ave}}^2}{\frac{\sum_{i \neq q} \sigma_{\alpha_i}^2}{N-1} \left(\frac{N-1}{M} \sum_{n=0}^{N-1} P_n^2 (\mu_{4,n} - 1) + N \sum_{n=0}^{N-1} P_n^2 - N^2 P_{\text{ave}}^2 \right) + \frac{\sigma_z^2}{M} N P_{\text{ave}}}$.

TABLE I
UNIFIED PROCESSING AND POWER-ALLOCATION RULES

Scheme	Processing	Optimal power allocation
Matched filtering	$H_s \leftarrow Y[n]X[n]^*$	$P_n = \frac{N P_{\text{ave}}}{b_n \sum_{n=1}^N b_n^{-1}},$ $b_n = \frac{1}{M} (\mu_{4,n} - 1) + \frac{N}{N-1}$
Reciprocal filtering	$H_s \leftarrow Y[n]/X[n]$	$P_n = \frac{N P_{\text{ave}} \sqrt{\nu_{-2,n}}}{\sum_{n=1}^N \sqrt{\nu_{-2,n}}}$

Proposition 2: Let $S \subseteq \{0, \dots, N-1\}$ with $\nu_{-2,n} = \nu_{-2}$ and $\mu_{4,n} = \mu_4$ for all $n \in S$. Then the optimal allocation satisfies $P_n = P_{n'}$ for all $n, n' \in S$.

Proof: Let $P_S = \sum_{n \in S} P_n$. For MF, the problem can be equivalently transformed into minimizing $\sum_{n \in S} P_n^2$ s.t. $\sum_{n \in S} P_n = P_S$. Since x^2 is convex,

$$\sum_{n \in S} P_n^2 \geq |S| \left(\frac{P_S}{|S|} \right)^2 = \frac{P_S^2}{|S|}, \quad (36)$$

with equality if and only if $P_n = P_S/|S|$ for all $n \in S$. For RF, the denominator depends on $\sum_{n \in S} 1/P_n$. Similarly, we have, $\sum_{n \in S} \frac{1}{P_n} \geq |S| \left(\frac{P_S}{|S|} \right)^{-1} = \frac{|S|^2}{P_S}$, with equality if and only if $P_n = P_S/|S|$ for all $n \in S$. In both cases the SINR numerator is unchanged, hence equal power on S is optimal. ■

1) *Matched Filtering:* Then, the optimal power allocation problem can be re-written as

$$\min_{\{P_n \geq 0\}} \sum_{n=1}^N b_n P_n^2, \quad \text{s.t.} \quad \sum_{n=1}^N P_n = N P_{\text{ave}}. \quad (37)$$

where $b_n = \frac{1}{M} (\mu_{4,n} - 1) + \frac{N}{N-1}$. The Lagrangian is

$$L = \sum_{n=1}^N b_n P_n^2 - \lambda \left(\sum_{n=1}^N P_n - N P_{\text{ave}} \right). \quad (38)$$

Taking the derivative with respect to P_n and setting it to zero yields $2b_n P_n - \lambda = 0$, $P_n^* = \frac{\lambda}{2b_n}$. Applying the power constraint, $\sum_{n=1}^N \frac{\lambda}{2b_n} = N P_{\text{ave}}$, $\lambda = \frac{2N P_{\text{ave}}}{\sum_{n=1}^N b_n^{-1}}$. Therefore, the optimal allocation is $P_i^* = \frac{N P_{\text{ave}}}{b_i \sum_{n=1}^N b_n^{-1}}$. Subcarriers with higher fourth moments, i.e., larger kurtosis, receive less power.

2) *Reciprocal Filtering:* For the reciprocal filter, the optimal power allocation is the solution to

$$\max_{\{P_n \geq 0\}} \frac{\left(\sum_{n=1}^N P_n \right)^2}{\sum_{n=1}^N \nu_{-2,n}/P_n} \quad \text{s.t.} \quad \sum_{n=1}^N P_n = N P_{\text{ave}}. \quad (39)$$

Using the Cauchy-Schwarz inequality, the minimum of $\sum_{n=1}^N \nu_{-2,i}/P_n$ under a sum constraint is achieved when

$$P_i^* = \frac{N P_{\text{ave}} \sqrt{\nu_{-2,i}}}{\sum_{n=1}^N \sqrt{\nu_{-2,n}}}. \quad (40)$$

Therefore, subcarriers with larger $\nu_{-2,i}$, i.e., more susceptible to noise amplification in RF, receive more power to compensate.

This section implies a "water-filling" like power allocation strategy for maximizing sensing performance. As summarized in Table I, the MF solution penalizes subcarriers with high kurtosis, whereas the RF solution allocates more power to subcarriers with a larger inverse second moment. These results yield closed-form guidelines for optimal power allocation in ISAC systems with arbitrary modulation constellations.

B. Joint Constellation Selection and Power Allocation for Sensing Improvement under Communication Guarantees

In this section, we analyze the joint constellation and power allocation under flat fading and frequency-selective channels. While the former admits a simple solution with at most three active constellations, the latter typically demands more diverse modulation across subcarriers.

1) *Flat Fading Channel*: We consider a scenario with a sufficiently large number of subcarriers, where the allocation of constellations for each subcarrier can be approximated by a continuous distribution over a set of candidate constellations. Let $\eta_j \in [0, 1]$ denote the proportion of subcarriers assigned to the j th candidate constellation. In the following, we rigorously prove that under identical channel gains (i.e., in a flat fading channel), the optimal solution requires at most three nonzero values of η_j . The flat fading assumption is valid for narrowband systems operating in environments with small delay spread.

By Proposition 2, all subcarriers using the same constellation are assigned equal power in the optimal solution. Then, when $N \rightarrow \infty$, it can be readily proved that the problem of (P1) can be equivalently transformed into

$$\max_{\boldsymbol{\eta}, \mathbf{P}} \text{SINR}_s, \quad (41a)$$

$$\text{s.t.} \quad \sum_{j=1}^J \eta_j = 1, \quad \eta_j \geq 0, \forall j, \quad (41b)$$

$$\sum_{j=1}^J \eta_j P_j = P_{\text{ave}}, \quad P_j \geq P_{j,\min}, \forall j, \quad (41c)$$

$$\sum_{j=1}^J \eta_j R_j \geq R_{\min}. \quad (41d)$$

$$\text{where } \boldsymbol{\eta} = [\eta_1, \dots, \eta_J], \quad \mathbf{P} = [P_1, \dots, P_J],$$

$$\text{SINR}_s = \frac{\sigma_{\alpha_q}^2 M N^2}{\sigma_{\alpha_q}^2 N \sum_{j=1}^J \eta_j \frac{\nu_{-2,j}}{P_j}} \text{ for RF, and } \text{SINR}_s = \frac{\sigma_{\alpha_q}^2 N^2 P_{\text{ave}}^2}{\sigma_{\alpha_q}^2 N^2 P_{\text{ave}}^2}$$

$$\frac{\sum_{i \neq q} \sigma_{\alpha_i}^2 \left[\frac{N}{M} \sum_{j=1}^J \eta_j P_j^2 (\mu_{4,j} - 1) + \frac{N^2 \sum_{j=1}^J \eta_j P_j^2 - N^2 P_{\text{ave}}^2}{N-1} \right] + \frac{\sigma_{\alpha_q}^2}{M} N P_{\text{ave}}}{\sigma_{\alpha_q}^2 N^2 P_{\text{ave}}^2}$$

for MF. Also, $R_j = \log_2 |\mathcal{C}_j|$.

Theorem 3: In (41), any optimal solution $\boldsymbol{\eta}^*$ is supported on at most three constellations, i.e.,

$$|\{j : \eta_j^* > 0\}| \leq 3. \quad (42)$$

Proof: Please refer to Appendix D. ■

Remark 2: The above result shows that any Pareto-optimal operating point can almost always be achieved by mixing at most three constellations. Intuitively, since the solution is a convex combination of constellation types in the 2-D space, Carathéodory's theorem [38] implies any optimum uses at most three extreme points, and if the rate constraint is inactive, at

most two. The case of three active constellations arises only when the rate constraint is exactly aligned with a convex combination of three different modulation rates, which is generally a measure-zero event in practice. Thus, for almost all feasible choices of the rate threshold, only two constellations are present in the optimal solution. This has significant engineering value: Instead of an exhaustive search over the entire J -dimensional simplex of constellation mixtures, it suffices to consider all $\binom{J}{2}$ possible triples and optimize their respective weights. The joint sensing-communication trade-off can therefore be efficiently implemented by continuously interpolating among three selected modulation formats. This greatly simplifies both offline system design and real-time adaptation, making the solution highly practical for deployment in ISAC systems.

To efficiently solve problem (41), we define the average power share of constellation j as $\theta_j \triangleq \eta_j P_j$. Then $P_j = \theta_j / \eta_j$ for any $\eta_j > 0$, and if $\eta_j = 0$ we set $\theta_j = 0$ (the choice of $P_j \geq 0$ is immaterial). With this substitution the constraints of (41) become

$$\sum_{j=1}^J \eta_j = 1, \quad \eta_j \geq 0; \quad \sum_{j=1}^J \theta_j = P_{\text{ave}}, \quad \theta_j \geq 0; \quad (43)$$

$$\sum_{j=1}^J \eta_j R_j \geq R_{\min}, \quad \eta_j P_{j,\min} \leq \theta_j \leq \eta_j P_{j,\max}, \forall j.$$

Here $P_{\max} > 0$ is a sufficiently large constant, whose sole purpose is to enforce $\eta_j = 0 \Rightarrow \theta_j = 0$.

For MF cases, noting $\sum_j \eta_j P_j^2 = \sum_j \frac{\theta_j^2}{\eta_j}$ and $N^2 \sum_j \eta_j P_j^2 - P_{\text{ave}}^2 = N^2 \sum_j \frac{\theta_j^2}{\eta_j} - P_{\text{ave}}^2$, the MF SINR denominator splits into a constant (independent of $(\boldsymbol{\eta}, \mathbf{y})$) plus a variable part. Dropping constants (which do not affect the maximizer), maximizing the MF SINR is equivalent to

$$\min_{\boldsymbol{\eta}, \boldsymbol{\theta}} \sum_{j=1}^J c_j \frac{\theta_j^2}{\eta_j} \quad \text{s.t.} \quad (43), \quad (44)$$

where $c_j = \left(\sum_{i \neq q} \sigma_{\alpha_i}^2 \right) \frac{N}{M} (\mu_{4,j} - 1) + \left(\sum_{i \neq q} \sigma_{\alpha_i}^2 \right) \frac{N^2}{N-1} > 0$.

For RF cases, since $\sum_j \eta_j \frac{\nu_{-2,j}}{P_j} = \sum_j \nu_{-2,j} \frac{\eta_j^2}{\theta_j}$, maximizing the RF SINR is equivalent to the convex program

$$\min_{\boldsymbol{\eta}, \boldsymbol{\theta}} \sum_{j=1}^J \nu_{-2,j} \frac{\eta_j^2}{\theta_j} \quad \text{s.t.} \quad (43). \quad (45)$$

Problems (44) and (45) are *strictly equivalent* to (41) under continuous power (with BER thresholds handled as $\theta_j \geq \eta_j P_{j,\min}$). Both are convex: each term η_j^2 / θ_j or θ_j^2 / η_j is quadratic-over-linear and the constraints are linear.

2) *Frequency-Selective Channel*: When subcarrier gains H_n vary across $n \in \{0, \dots, N-1\}$, the three-constellation principle in Theorem 3 no longer holds. Each subcarrier should choose its constellation according to its local channel quality. Define the power relevant variable

$$\kappa_{n,j} \triangleq \chi_{n,j} p_{n,j}, \quad (46)$$

so that $p_{n,j}$ is the transmit power when $\chi_{n,j} = 1$ (otherwise $p_{n,j}$ is immaterial and $\kappa_{n,j} = 0$). For a target BER, denote the per-subcarrier minimum power by $P_{n,j}^{\min} \triangleq P_j^{\min}(H_n)$, and let P_{\max} be a loose upper bound. For MF-based sensing, the coefficient

$a_j = \left(\sum_{i \neq q} \sigma_{\alpha_i}^2 \right) \frac{N}{M} (\mu_{4,j} - 1) + \left(\sum_{i \neq q} \sigma_{\alpha_i}^2 \right) \frac{N^2}{N-1} > 0$ collects the modulation-dependent moments.

Then, maximizing MF-SINR is equivalent to the following mixed-integer quadratic-over-linear (QOL) program:

$$\min_{\chi, \kappa} \sum_{n=0}^{N-1} \sum_{j=1}^J a_j \frac{\kappa_{n,j}^2}{\chi_{n,j}}, \quad (47a)$$

$$\text{s.t.} \quad \sum_{j=1}^J \chi_{n,j} = 1, \quad \chi_{n,j} \in \{0, 1\}, \quad \forall n, \quad (47b)$$

$$\frac{1}{N} \sum_{n=0}^{N-1} \sum_{j=1}^J \kappa_{n,j} = P_{\text{ave}}, \quad \kappa_{n,j} \geq 0, \quad (47c)$$

$$\frac{1}{N} \sum_{n=0}^{N-1} \sum_{j=1}^J \chi_{n,j} R_j \geq R_{\text{min}}, \quad (47d)$$

$$\chi_{n,j} P_{n,j}^{\text{min}} \leq \kappa_{n,j} \leq \chi_{n,j} P_{\text{max}}, \quad \forall n, j. \quad (47e)$$

The perspective $\kappa_{n,j}^2 / \chi_{n,j}$ is jointly convex on $\{\chi_{n,j} > 0, \kappa_{n,j} \geq 0\}$ and enforces $\kappa_{n,j} = 0$ if $\chi_{n,j} = 0$ via (47e). The problem admits an exact reformulation as a mixed-integer second-order cone program (MISOCP).

We introduce the dual variables $\psi_{\mathcal{L}} \in \mathbb{R}$ for (47c) and $\lambda_{\mathcal{L}} \geq 0$ for (47d). Dropping constants, the MF Lagrangian reads

$$\begin{aligned} \mathcal{L}_{\text{MF}}(\chi, \kappa; \psi_{\mathcal{L}}, \lambda_{\mathcal{L}}) &= \sum_{n,j} a_j \frac{\kappa_{n,j}^2}{\chi_{n,j}} - \psi_{\mathcal{L}} \left(\sum_{n,j} \kappa_{n,j} - NP_{\text{ave}} \right) \\ &\quad + \lambda_{\mathcal{L}} \left(R_{\text{min}} - \frac{1}{N} \sum_{n,j} \chi_{n,j} R_j \right). \end{aligned} \quad (48)$$

We now design a low-complexity scheme by moving the coupling constraints into the objective via $(\psi_{\mathcal{L}}, \lambda_{\mathcal{L}})$ so that, for fixed prices, the N subcarriers decouple.

a) Inner layer update.: For a fixed $(\psi_{\mathcal{L}}, \lambda_{\mathcal{L}})$ and an active pair (n, j) (i.e., $\chi_{n,j} = 1$), minimizing w.r.t. $\kappa_{n,j}$ over the interval $[P_{n,j}^{\text{min}}, P_{\text{max}}]$ yields the one-dimensional convex quadratic

$$\min_{P_{n,j}^{\text{min}} \leq \kappa \leq P_{\text{max}}} a_j \kappa^2 - \psi_{\mathcal{L}} \kappa, \quad (49)$$

whose optimal value is the reduced cost

$$\phi_{n,j}(\psi_{\mathcal{L}}) = \begin{cases} a_j (P_{n,j}^{\text{min}})^2 - \psi_{\mathcal{L}} P_{n,j}^{\text{min}}, & \frac{\psi_{\mathcal{L}}}{2a_j} \leq P_{n,j}^{\text{min}}, \\ -\frac{\psi_{\mathcal{L}}^2}{4a_j}, & P_{n,j}^{\text{min}} \leq \frac{\psi_{\mathcal{L}}}{2a_j} \leq P_{\text{max}}, \\ a_j P_{\text{max}}^2 - \psi_{\mathcal{L}} P_{\text{max}}, & \frac{\psi_{\mathcal{L}}}{2a_j} \geq P_{\text{max}}. \end{cases} \quad (50)$$

Substituting $\phi_{n,j}(\psi_{\mathcal{L}})$ back into (48) eliminates κ and leaves a linear form in χ : $\sum_{n,j} \chi_{n,j} (\phi_{n,j}(\psi_{\mathcal{L}}) - \frac{\lambda_{\mathcal{L}}}{N} R_j) + \psi_{\mathcal{L}} NP_{\text{ave}} + \lambda_{\mathcal{L}} R_{\text{min}}$. Due to constraints in (47b), the minimum over χ is attained at a simplex vertex, i.e.,

$$j_n \in \arg \min_j \left\{ \phi_{n,j}(\psi_{\mathcal{L}}) - \frac{\lambda_{\mathcal{L}}}{N} R_j \right\}, \quad \chi_{n,j_n} = 1, \quad \chi_{n,j \neq j_n} = 0. \quad (51)$$

Given $\{j_n\}$, under the Lagrangian relaxation the per-subcarrier power update is separable and admits a clamped closed form:

$$\kappa_n^*(\psi_{\mathcal{L}}) = \min \left\{ P_{\text{max}}, \max \left\{ P_{n,j_n}^{\text{min}}, \frac{\psi_{\mathcal{L}}}{2a_{j_n}} \right\} \right\}. \quad (52)$$

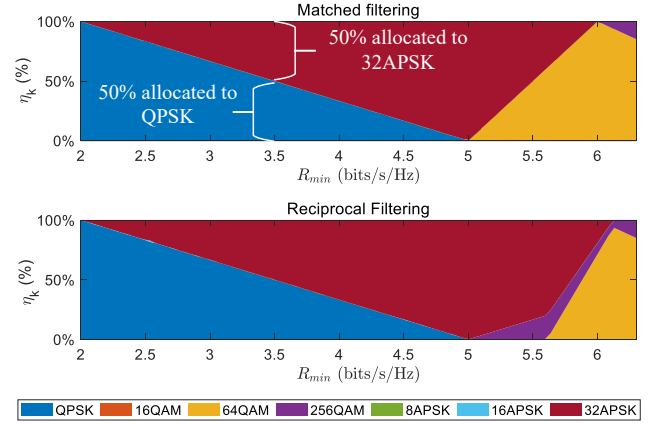


Fig. 3. Constellation proportions versus R_{min} ($P_{\text{ave}} = 6$).

b) Outer layer update.: Let $\bar{R} = \frac{1}{N} \sum_n R_{j_n}$ be the achieved average rate and $S_y = \sum_n \kappa_n^*$ the total power returned by (52). $\psi_{\mathcal{L}}$ and $\lambda_{\mathcal{L}}$ are updated by a projected subgradient,

$$\psi_{\mathcal{L}}^{(t+1)} = \psi_{\mathcal{L}}^{(t)} + \psi_t \left(NP_{\text{ave}} - \sum_n \kappa_n^*(\psi_{\mathcal{L}}^{(t)}) \right) \quad (53)$$

and

$$\lambda_{\mathcal{L}}^{(t+1)} = \left[\lambda_{\mathcal{L}}^{(t)} + \psi_t (R_{\text{min}} - \bar{R}^{(t)}) \right]_+, \quad (54)$$

where $\psi_t > 0$. Combining (51)-(54) yields a scalable bilevel scheme that preserves the binary selection $\chi_{n,j} \in \{0, 1\}$, satisfies the BER lower bounds, and computes κ in closed form at every iteration.

The RF case uses the same constraint set (47b)-(47e) and replaces the objective by $\frac{\sigma_z^2}{MN} \sum_{n,j} \nu_{-2,j} \frac{\chi_{n,j}^2}{\kappa_{n,j}}$. Proceeding identically, first eliminating κ to obtain a per-pair reduced cost and then applying the one-hot rule (51), leads to an analogous closed-form power update. To save space, we omit the RF algebra; it is entirely similar.

V. SIMULATIONS AND EXPERIMENTS

Using numerical simulation and experimental results, we have studied the fundamental characteristics of constellation combination of ISAC systems. The system parameters are given as follows: the frequency $f^c = 2.45$ GHz; the bandwidth $B = 20$ MHz; the noise power -100 dB, subcarrier number $N = 64$, number of coherent processing symbols $M = 16$, the threshold of BER is set as 10^{-4} .

A. Simulations: Tradeoffs between Sensing and Communication

Fig. 3 illustrates the optimal constellation mixture η as a function of the minimum rate guarantee R_{min} for identical subcarrier channel gains, under both MF and RF processing, where the y-axis reports the subcarrier proportion. Specifically, when the rate constraint is 3.5 bits/s/Hz, the optimal constellation mixture for both MF and RF consists of 50% QPSK and 50% 32APSK. Consistent with Theorem 3 under the flat fading channel, across almost the entire range of R_{min} , the optimizer activates no more than three constellations at a time. For mild rate requirements, the solution concentrates on low-order constellations (predominantly QPSK) to suppress MF sidelobes and reduce the RF noise-variance term. As R_{min}

tightens, the mixture shifts monotonically toward higher-order constellations (e.g., 32APSK/64QAM), reducing the share of low-order formats to meet the rate while maintaining sensing quality. Under frequency-flat channels, MF and RF show almost identical switching thresholds and piecewise-linear transitions, indicating essentially the same constellation mixture.

Fig. 4 shows the optimal joint constellation selection and power allocation over a frequency-selective channel ($N = 64$, $M = 16$, $R_{\min} = 6$ bits/s/Hz). The red curve gives the subcarrier gains $|H_n|^2$ sorted in descending order, while bar colors indicate the chosen constellation and bar heights the allocated power P_n . For both MF and RF (c.f. Fig. 4(a) and Fig. 4(b)), subcarriers with larger $|H_n|^2$ are mapped to higher-order constellations, exploiting the strong channels to meet the communication rate requirements with less power, whereas the subcarriers with weaker channel gain are assigned lower-order constellations to preserve the sensing metric, i.e., reduced MF sidelobes or smaller RF noise variance with only a modest rate penalty. Moreover, within any contiguous block employing the same constellation, the optimal per-subcarrier powers equalize at the BER threshold, in agreement with Proposition 2. It is noted that only subcarriers near block boundaries show increased P_n to reach this threshold, after which additional power yields little benefit and is therefore not allocated. The MF and RF solutions share a similar block structure and power allocation trends, differing only by small boundary offsets.

Fig. 5 illustrates that range RMSE versus SNR for both MF and RF. In Fig. 5(a), with optimal power allocation and varying constellation mixtures, MF attains lower RMSE at low SNR, whereas RF becomes superior at high SNR. This crossover arises because reciprocal weighting in RF increases effective noise variance at low SNR, especially when the mixture includes constellations without a constant envelope such as 16QAM, while MF is limited at high SNR by a sidelobe floor. A higher fraction of 16QAM consistently degrades sensing for both criteria: RMSE is largest with 100% 16QAM, intermediate with 50% QPSK and 50% 16QAM, and smallest with 100% QPSK. Fig. 5(b) shows that for a fixed 50% QPSK and 50% 16QAM mixture, the optimal power allocation consistently outperforms both random allocation and the communications water-filling baseline. The gain is most pronounced for MF at low SNR and remains substantial for RF at high SNR.

Fig. 6 plots the sensing metric versus the minimum rate R_{\min} at fixed transmit power. For MF reported as SINR and RF reported as SNR, the curves decrease monotonically with R_{\min} , which quantifies the sensing and communication tradeoff. RF attains a higher metric than MF across the entire range. The proposed heuristic remains close to the MISOCP benchmark with a bounded gap that narrows as R_{\min} increases: about 2 to 3 dB for MF and about 1 to 2 dB for RF at small R_{\min} . The residual gap arises from the fixed approximation used to linearize the BER and sensing terms and from using an alternating update of the constellation mixture and the per-subcarrier powers rather than a single joint solve.

B. Over-the-air Experiment Results

As shown in Fig. 7, the field trial was conducted in a street-canyon environment. An ISAC node built with ADALM-Pluto

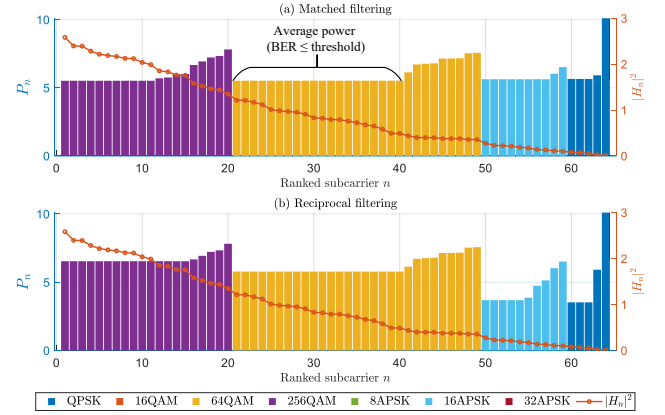


Fig. 4. Constellation results per subcarrier allocation with $R_{\min} = 6$ bps/Hz and $N = 64$, $M = 16$.

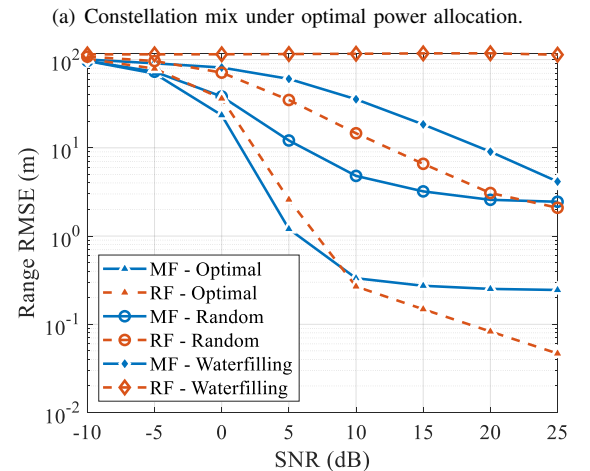
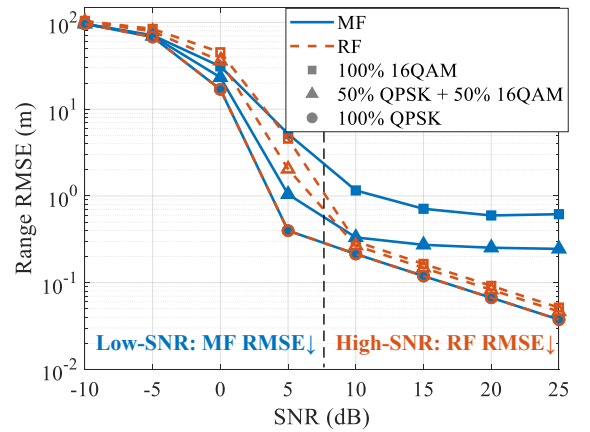


Fig. 5. Range RMSE comparison for MF and RF.

SDRs was installed on a rooftop, with a co-located receiver forming a monostatic sensing channel, while a second Pluto placed down-range acted as the communication receiver. The dashed line indicates the propagation path toward the building façade that served as the radar target (about 132.6 m). During the experiments we transmitted OFDM frames with the proposed constellation selection strategy active at the transmitter. For each configuration we recorded sensing outputs including the range profile, the target distance estimate, and aggregate sens-

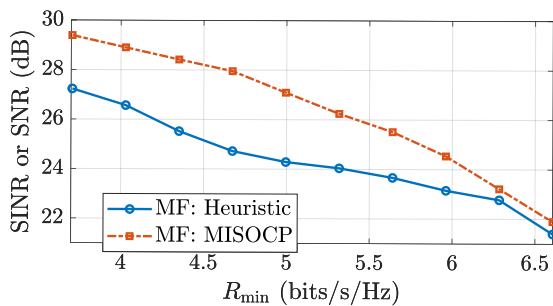


Fig. 6. Tradeoff between sensing and communications in (P1).



Fig. 7. Scenario of experiments (google maps).

ing metrics, together with communication outcomes including throughput and bit error rate. This controlled protocol enables a fair comparison of ranging accuracy and communication quality and isolates the effect of constellation selection.

Fig. 8 shows range profiles (magnitude in dB) for MF and RF under three constellation mixes, including 100% QPSK, 50% QPSK and 50% 16QAM, as well as 100% 16QAM. As the share of 16QAM increases, the MF sidelobe level rises markedly across the entire delay axis, producing a pronounced clutter bump (e.g., near 50-80 m) and a monotonic degradation of the peak-to-sidelobe ratio (PSLR) around the true target. This follows from the larger amplitude variance / higher fourth-order moment of non-constant-envelope 16QAM, which injects more off-peak correlation energy that MF passes to the output. RF exhibits the same qualitative trend but with a milder increase, because its reciprocal weighting attenuates part of the off-peak energy while suffering a modest rise in effective noise-power variance. Overall, higher 16QAM fractions elevate sidelobes (MF more than RF) and reduce PSLR, while the target peak location remains unchanged.

As shown in Fig. 9, we compare coherent integration over $M \in \{10, 100, 500\}$ symbols for both the MF and the RF processor. The range peak at 132.6 m is preserved across all cases, while the sidelobe floor decreases with M in accordance with the coherent-processing law $10 \log_{10} M$. Specifically, increasing M from 10 to 100 yields an approximate 10 dB reduction of sidelobes, and from 100 to 500 yields an additional 7 dB reduction of sidelobes. This matches the theoretical expression derived for the MF sidelobe level. The trends for RF are consistent: enlarging M effectively mitigates the excess noise introduced by the random communication waveform, leading to noticeably lower sidelobes at larger M . Overall, the measurements indicate a high-SNR regime where sidelobe suppression

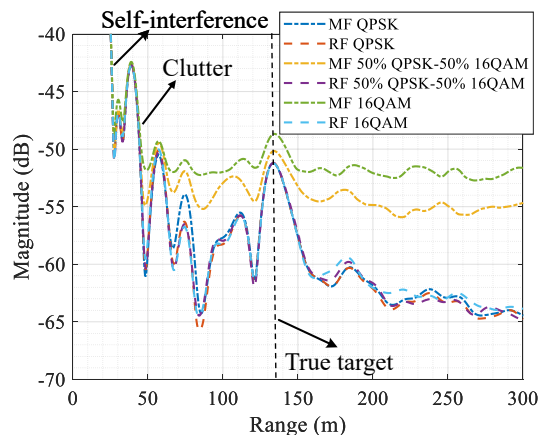


Fig. 8. Sensing profile versus constellation mixes for MF and RF.

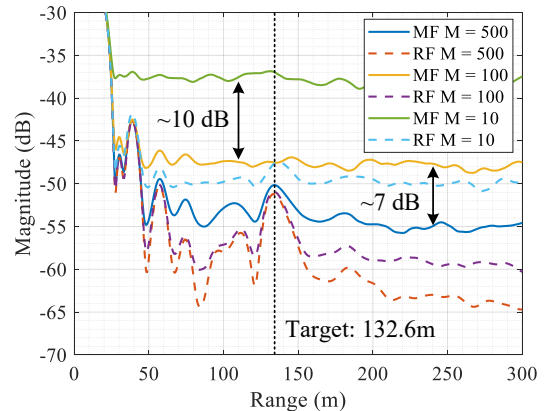


Fig. 9. Coherent signal processing gain versus coherent symbol number.

scales predictably with M , corroborating the analysis.

Fig. 10 shows the received I/Q scatter (constellation diagram) for a mixed-constellation OFDM frame in which some subcarriers use QPSK and others 16QAM. The detected point clouds align tightly with the reference constellation markers, indicating well-separated decision regions and bounded error vector magnitude (EVM) for both formats. Since the receiver knows the per-subcarrier constellation map (e.g., via pre-designed protocol and control signaling), it applies the appropriate slicer on each tone and decodes reliably despite the heterogeneous modulation. This confirms that the proposed mixed-constellation allocation, used to benefit sensing, does not compromise communication demodulation performance.

Fig. 11 plots the sensing performance versus the QPSK fraction in a mixed QPSK and 16QAM frame where the remaining symbols are 16QAM. As the QPSK fraction increases, effective SINR rises and ranging error falls for both MF and RF; the improvement is especially marked for MF because 16 QAM's amplitude dispersion elevates sidelobe/clutter power and inflates estimator variance. It can be found that replacing 16QAM with the constant-envelope QPSK suppresses these sidelobes and sharply improves MF accuracy. RF shows a much milder dependence on the mix because its reciprocal weighting already mitigates symbol-induced sidelobes, and thus its improvement with more QPSK comes mainly from a reduction in the effective noise-power term. As the frame approaches all-QPSK, both MF

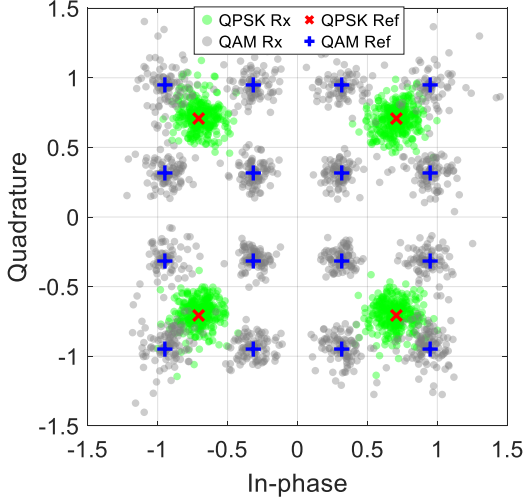


Fig. 10. Received I/Q scatter of constellation diagram at the communication receiver.

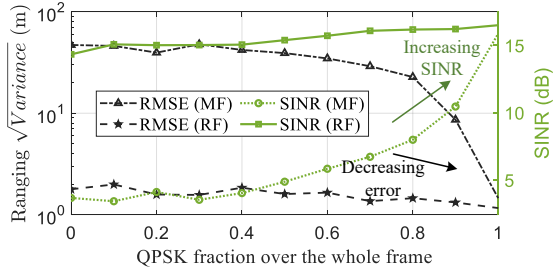


Fig. 11. Sensing performance versus the QPSK fraction within the OFDM frame (remaining symbols use 16QAM), under uniform power allocation.

and RF achieve their best accuracy.

Fig. 12 plots BER (left axis, blue) and aggregate throughput (right axis, red) versus the fraction of QPSK used across all subcarriers in a frame. Throughput is reported as $R_{\text{com}}(1 - \text{BER})$. As the QPSK fraction over the whole frame increases, the BER decreases monotonically ($\approx 10^{-2} \rightarrow 10^{-4}$), reflecting the higher robustness of the lower-order constellation. However, as the concomitant loss of spectral efficiency dominates, the net throughput declines steadily because the BER reduction is insufficient to offset the rate penalty from replacing higher-order modulation with QPSK. This trend highlights the expected reliability-rate tradeoff under the tested SNR and coding settings. As the QPSK fraction changes, Fig. 13 reveals a tradeoff between sensing SINR output after receive filtering and achievable throughput, evidencing that constellation selection governs the sensing-communication balance.

VI. CONCLUSION

This paper developed a standards-compatible, OFDM-based ISAC framework that makes the sensing-communication tradeoff explicit through constellation combination and power shaping. Treating payload symbols as a random process, we established moment-driven sensing laws: MF sidelobes are governed by the per-subcarrier fourth moment, while RF noise amplification is governed by the inverse second moment. The analysis extends to multi-symbol coherent integration, predicts the expected processing gain, and enables super-resolution delay estimation.

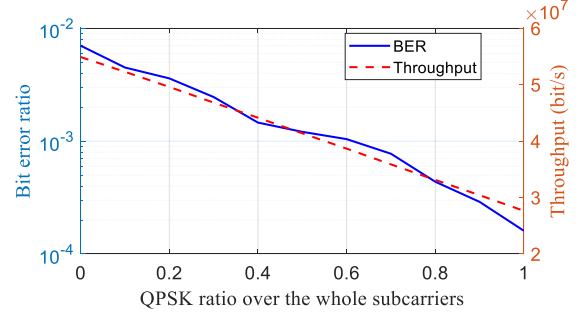


Fig. 12. Communication BER and throughput versus QPSK fraction (remaining symbols use 16QAM).

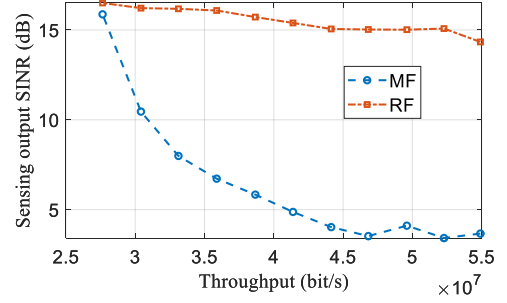


Fig. 13. Tradeoff between sensing output after receive filtering and communication throughput.

Guided by these laws, we proposed a low-complexity co-design that retains a finite, off-the-shelf constellation set and optimally shapes power subject to rate and BER constraints. We proved structural optimality in flat fading channels, any Pareto point activates at most three constellations, and provided convex-equivalent formulations with an exact MISOCP benchmark. For frequency-selective channels, a bilevel algorithm with closed-form inner updates preserves binary constellation decisions and attains near-optimal performance at a fraction of the cost. Extensive simulations and experiments corroborate the analysis: Mixed-constellation frames demodulate reliably with appropriate subcarrier power control; increasing the constant-envelope share suppresses sidelobes; and performance crosses over from MF at low SNR to RF at high SNR. These results show that constellation-aware power shaping is a practical, standards-compliant lever for ISAC.

APPENDIX A: PROOF OF PROPOSITION 1

According to the definition, r_k can be further expressed as

$$\begin{aligned}
 r_k &= \sum_{t=0}^{N-1} \left(\frac{1}{\sqrt{N}} \sum_{n=0}^{N-1} \sqrt{P_n} s_n^* e^{-j\frac{2\pi}{N}nt} \right) \\
 &\quad \left(\frac{1}{\sqrt{N}} \sum_{n'=0}^{N-1} \sqrt{P_{n'}} s_{n'} e^{j\frac{2\pi}{N}n'(t+k)} \right) \\
 &= \frac{1}{N} \sum_{n=0}^{N-1} \sum_{n'=0}^{N-1} \sqrt{P_n P_{n'}} s_n^* s_{n'} e^{j\frac{2\pi}{N}n'k} \sum_{t=0}^{N-1} e^{j\frac{2\pi}{N}(n'-n)t} \\
 &= \sum_{n=0}^{N-1} P_n |s_n|^2 e^{j\frac{2\pi}{N}kn}.
 \end{aligned} \tag{55}$$

Then, we have

$$\begin{aligned} |r_k|^2 &= \left| \sum_{n=0}^{N-1} P_n |s_n|^2 e^{j \frac{2\pi}{N} kn} \right|^2 \\ &= \sum_{n=0}^{N-1} \sum_{n'=0}^{N-1} P_n P_{n'} |s_n|^2 |s_{n'}|^2 e^{j \frac{2\pi}{N} k(n-n')}. \end{aligned} \quad (56)$$

Taking expectations and splitting the double sum into diagonal ($n = n'$) and off-diagonal ($n \neq n'$) parts yields

$$\mathbb{E}[|r_k|^2] = \sum_{n=0}^{N-1} \mu_{4,n} P_n^2 + \sum_{\substack{n, n'=0 \\ n \neq n'}}^{N-1} P_n P_{n'} e^{j \frac{2\pi}{N} k(n-n')}, \quad (57)$$

where we used $\mathbb{E}[|s_n|^4] = \mu_{4,n}$ and, by independence and unit-power normalization, $\mathbb{E}[|s_n|^2 |s_{n'}|^2] = 1$ for $n \neq n'$.

Summing (57) over $k = 1, \dots, N-1$, the first (diagonal) term is k -independent and contributes

$$\sum_{k=1}^{N-1} \sum_{n=0}^{N-1} \mu_{4,n} P_n^2 = (N-1) \sum_{n=0}^{N-1} \mu_{4,n} P_n^2. \quad (58)$$

For the off-diagonal case $n \neq n'$, the independence of s_n and $s_{n'}$ implies $\mathbb{E}[|s_n|^2 |s_{n'}|^2] = 1$, resulting in the term $\sum_{n \neq n'} P_n P_{n'} e^{j \frac{2\pi}{N} k(n-n')}$. Combining these results, the expectation of $|r_k|^2$ can be expressed as

$$\mathbb{E}[|r_k|^2] = \sum_{n=0}^{N-1} P_n^2 \mu_{4,n} + \sum_{n \neq n'} P_n P_{n'} e^{j \frac{2\pi}{N} k(n-n')}. \quad (59)$$

Noting that $\left| \sum_{n=0}^{N-1} P_n e^{j \frac{2\pi}{N} kn} \right|^2 = \sum_n P_n^2 + \sum_{n \neq n'} P_n P_{n'} e^{j \frac{2\pi}{N} k(n-n')}$, we have $\sum_{k=1}^{N-1} \sum_{n \neq n'} P_n P_{n'} e^{j \frac{2\pi}{N} k(n-n')} = \sum_{k=1}^{N-1} \left| \sum_{n=0}^{N-1} P_n e^{j \frac{2\pi}{N} kn} \right|^2 - (N-1) \sum_n P_n^2$. Combining with the diagonal part yields $(N-1) \sum_n (\mu_{4,n} - 1) P_n^2 + \sum_{k=1}^{N-1} \left| \sum_{n=0}^{N-1} P_n e^{j \frac{2\pi}{N} kn} \right|^2$, which leads to the ESL formula after applying Parseval theorem.

APPENDIX B: PROOF OF THEOREM 1

The expected ACF at lag k is

$$\mathbb{E}[\bar{r}_k] = \sum_{n=0}^{N-1} P_n e^{j \frac{2\pi}{N} nk}, \quad (60)$$

since $\mathbb{E}[|s_n^{(m)}|^2] = 1$. Therefore, the mean of \bar{r}_k remains unchanged compared to the single-symbol case. That is, the mean is invariant under averaging.

To compute $\mathbb{E}[|\bar{r}_k|^2]$, we analyze the variance of $r_k^{(m)}$:

$$\text{Var}(r_k^{(m)}) = \mathbb{E}[|r_k^{(m)}|^2] - |\mathbb{E}[r_k^{(m)}]|^2, \quad (61)$$

$$\mathbb{E}[|r_k^{(m)}|^2] = \sum_{n=0}^{N-1} P_n^2 \mu_{4,n} + \sum_{n \neq n'} P_n P_{n'} e^{j \frac{2\pi}{N} k(n-n')}, \quad (62)$$

$$|\mathbb{E}[r_k^{(m)}]|^2 = \left| \sum_{n=0}^{N-1} P_n e^{j \frac{2\pi}{N} nk} \right|^2. \quad (63)$$

Using the identity

$$\sum_{n \neq n'} P_n P_{n'} e^{j \frac{2\pi}{N} k(n-n')} = \left| \sum_{n=0}^{N-1} P_n e^{j \frac{2\pi}{N} nk} \right|^2 - \sum_{n=0}^{N-1} P_n^2, \quad (64)$$

we simplify the variance as

$$\text{Var}(r_k^{(m)}) = \sum_{n=0}^{N-1} P_n^2 (\mu_{4,n} - 1). \quad (65)$$

Since the autocorrelations $r_k^{(m)}$ across different symbols are independent, the variance of their average is reduced by a factor of $1/M$, i.e.,

$$\text{Var}(\bar{r}_k) = \frac{1}{M} \text{Var}(r_k^{(m)}). \quad (66)$$

This implies that the variance of the autocorrelation follows directly from the single-symbol case, scaled by $1/M$ due to averaging.

Therefore, the second-order moment of the averaged ACF becomes

$$\mathbb{E}[|\bar{r}_k|^2] = \frac{1}{M} \sum_{n=0}^{N-1} P_n^2 (\mu_{4,n} - 1) + \left| \sum_{n=0}^{N-1} P_n e^{j \frac{2\pi}{N} nk} \right|^2. \quad (67)$$

Using Parseval's identity,

$$\sum_{k=0}^{N-1} \left| \sum_{n=0}^{N-1} P_n e^{j \frac{2\pi}{N} nk} \right|^2 = N \sum_{n=0}^{N-1} P_n^2, \quad (68)$$

we extract the sidelobe power as

$$\sum_{k=1}^{N-1} \left| \sum_{n=0}^{N-1} P_n e^{j \frac{2\pi}{N} nk} \right|^2 = N \sum_{n=0}^{N-1} P_n^2 - \left(\sum_{n=0}^{N-1} P_n \right)^2. \quad (69)$$

Thus, the integrated sidelobe over nonzero lags is

$$\sum_{k=1}^{N-1} \mathbb{E}[|\bar{r}_k|^2] = \frac{N-1}{M} \sum_{n=0}^{N-1} P_n^2 (\mu_{4,n} - 1) + N \sum_{n=0}^{N-1} P_n^2 - \left(\sum_{n=0}^{N-1} P_n \right)^2. \quad (70)$$

Substituting these into the SINR definition completes the proof.

APPENDIX C: PROOF OF THE RF SNR (UNITARY DFT)

First, for single symbol ($M = 1$), RF per subcarrier is represented by

$$\hat{Y}_m[n] = \frac{Y_m[n] X_m[n]^*}{|X_m[n]|^2} = \sum_{q=1}^Q \alpha_q e^{-j \frac{2\pi}{N} n \tau_q} + \underbrace{\frac{Z_m[n]}{X_m[n]}}_{\triangleq \tilde{Z}_m[n]}. \quad (71)$$

Conditioned on $X_m[n]$, $\tilde{Z}_m[n] \sim \mathcal{CN}(0, \sigma_z^2 / |X_m[n]|^2)$, hence

$$\mathbb{E}[|\tilde{Z}_m[n]|^2] = \sigma_z^2 \mathbb{E}[|X_m[n]|^{-2}] = \sigma_z^2 \frac{\nu-2, n}{P_n}. \quad (72)$$

Transforming back to time via the unitary IDFT,

$$\tilde{y}_m[t] = \frac{1}{\sqrt{N}} \sum_{n=0}^{N-1} \hat{Y}_m[n] e^{j \frac{2\pi}{N} nt} = \sum_{q=1}^Q \alpha_q \mathcal{D}_N(t - \tau_q) + w_m[t], \quad (73)$$

where $\mathcal{D}_N(\cdot)$ is the periodic Dirichlet kernel with $\mathcal{D}_N(0) \triangleq \sqrt{N}$, and $w_m[t] = \frac{1}{\sqrt{N}} \sum_{n=0}^{N-1} \tilde{Z}_m[n] e^{j \frac{2\pi}{N} nt}$, where $\text{Var}(w_m[t]) = \frac{1}{N} \sum_{n=0}^{N-1} \sigma_z^2 \frac{\nu-2, n}{P_n}$. At the main peak ($t = \tau_q$ and $\tau_q \in \mathbb{Z}$), the signal power is $|\alpha_q|^2 |\mathcal{D}_N(0)|^2 = |\alpha_q|^2 N$. Therefore,

$$\text{SNR}_{q, M=1}^{\text{RF}} = \frac{\sigma_{\alpha_q}^2 N^2}{\sigma_z^2 \sum_{n=0}^{N-1} \frac{\nu-2, n}{P_n}}. \quad (74)$$

Considering coherent averaging over M symbols, the time-domain noise after IDFT, $\bar{w}[t] = \frac{1}{\sqrt{N}} \sum_n \bar{Z}[n] e^{j\frac{2\pi}{N}nt}$, has

$$\text{Var}(\bar{w}[t]) = \frac{1}{N} \sum_{n=0}^{N-1} \frac{1}{M} \sigma_z^2 \frac{\nu_{-2,n}}{P_n} = \frac{\sigma_z^2}{MN} \sum_{n=0}^{N-1} \frac{\nu_{-2,n}}{P_n}. \quad (75)$$

The peak signal power remains $\sigma_{\alpha_q}^2 N$, hence

$$\text{SNR}_q^{\text{RF}} = \frac{\sigma_{\alpha_q}^2 N^2 M}{\sigma_z^2 \sum_{n=0}^{N-1} \frac{\nu_{-2,n}}{P_n}} \quad (76)$$

This thus completes the proof.

APPENDIX D: PROOF OF THEOREM 3

The feasible set is defined by

$$\sum_{j=1}^J \eta_j = 1, \quad \sum_{j=1}^J \eta_j P_j = P_{\text{ave}}, \quad \sum_{j=1}^J \eta_j R_j \geq R_{\text{min}}, \quad \eta_j \geq 0. \quad (77)$$

At any vertex, the number of active (equality) constraints equals the number of variables J . If the rate constraint is inactive, only two equalities are tight, so at most two η_j are nonzero. If the rate constraint is active, then three equalities are tight, so at most three η_j are nonzero. Since the objective is a linear-fractional function of $\boldsymbol{\eta}$ with any fixed transmit power, the optimum is always attained at a vertex [38]. Thus, the optimal solution involves at most two active constellation types, or three if the rate constraint is active.

REFERENCES

- [1] Y. Lu, H. Ma, E. Smart, and H. Yu, "Real-time performance-focused localization techniques for autonomous vehicle: A review," *IEEE Transactions on Intelligent Transportation Systems*, vol. 23, no. 7, pp. 6082–6100, 2021.
- [2] Z. Zhang, F. Wen, Z. Sun, X. Guo, T. He, and C. Lee, "Artificial intelligence-enabled sensing technologies in the 5g/internet of things era: from virtual reality/augmented reality to the digital twin," *Advanced Intelligent Systems*, vol. 4, no. 7, p. 2100228, 2022.
- [3] J. A. Zhang *et al.*, "An overview of signal processing techniques for joint communication and radar sensing," *IEEE J. Sel. Top. Signal Process.*, vol. 15, no. 6, pp. 1295–1315, 2021.
- [4] A. Liu *et al.*, "A survey on fundamental limits of integrated sensing and communication," *IEEE Commun. Surveys Tuts.*, vol. 24, no. 2, pp. 994–1034, Nov. 2022.
- [5] K. Meng, Q. Wu, W. Chen, and D. Li, "Sensing-assisted communication in vehicular networks with intelligent surface," *IEEE Trans. Veh. Technol.*, vol. 73, no. 1, pp. 876–893, 2024.
- [6] X. Wang, Z. Fei, P. Liu, J. A. Zhang, Q. Wu, and N. Wu, "Sensing-aided covert communications: Turning interference into allies," *IEEE Trans. Wireless Commun.*, vol. 23, no. 9, pp. 10726–10739, 2024.
- [7] T. Ma, Y. Xiao, X. Lei, and M. Xiao, "Integrated sensing and communication for wireless extended reality (xr) with reconfigurable intelligent surface," *IEEE Journal of Selected Topics in Signal Processing*, vol. 17, no. 5, pp. 980–994, 2023.
- [8] Y. Cui, F. Liu, X. Jing, and J. Mu, "Integrating sensing and communications for ubiquitous IoT: Applications, trends, and challenges," *IEEE Net.*, vol. 35, no. 5, pp. 158–167, Sep./Oct. 2021.
- [9] K. Meng *et al.*, "Integrated sensing and communication meets smart propagation engineering: Opportunities and challenges," *IEEE Network*, vol. 39, no. 2, pp. 278–285, 2025.
- [10] K. Han *et al.*, "MIMO-OFDM signaling design for noncoherent distributed ISAC systems," *IEEE Trans. Wireless Commun.*, vol. 25, pp. 7792–7808, 2026.
- [11] M. Hua *et al.*, "3D multi-target localization via intelligent reflecting surface: Protocol and analysis," *IEEE Trans. Wireless Commun.*, 2024.
- [12] X. Wang, Z. Fei, J. A. Zhang, and J. Xu, "Partially-connected hybrid beamforming design for integrated sensing and communication systems," *IEEE Trans. Commun.*, vol. 70, no. 10, pp. 6648–6660, 2022.
- [13] S. Lu *et al.*, "Integrated sensing and communications: Recent advances and ten open challenges," *IEEE Internet Things J.*, vol. 11, no. 11, pp. 19 094–19 120, 2024.
- [14] K. Meng, C. Masouros, A. P. Petropulu, and L. Hanzo, "Cooperative ISAC networks: Opportunities and challenges," *IEEE Wireless Communications*, vol. 32, no. 3, pp. 212–219, 2025.
- [15] —, "Cooperative ISAC networks: Performance analysis, scaling laws, and optimization," *IEEE Trans. Wireless Commun.*, vol. 24, no. 2, pp. 877–892, 2025.
- [16] K. Han, K. Meng, X.-Y. Wang, and C. Masouros, "Network-level ISAC design: State-of-the-art, challenges, and opportunities," *IEEE Journal of Selected Topics in Electromagnetics, Antennas and Propagation*, pp. 1–18, 2025.
- [17] K. Meng, C. Masouros, G. Chen, and F. Liu, "Network-level integrated sensing and communication: Interference management and BS coordination using stochastic geometry," *IEEE Trans. Wireless Commun.*, vol. 23, no. 12, pp. 19 365–19 381, 2024.
- [18] Z. Wei *et al.*, "Integrated sensing and communication signals toward 5G-A and 6G: A survey," *IEEE Internet Things J.*, vol. 10, no. 13, pp. 11 068–11 092, 2023.
- [19] S. Lu, F. Liu, F. Dong, Y. Xiong, J. Xu, Y.-F. Liu, and S. Jin, "Random ISAC signals deserve dedicated precoding," *IEEE Trans. Signal Processing*, vol. 72, pp. 3453–3469, 2024.
- [20] M. A. Chitre, J. Tian, and H. Vishnu, "On ambiguity function shaping for broadband constant-modulus signals," *Signal Processing*, vol. 166, p. 107224, 2020.
- [21] 3GPP, "Nr: physical channels and modulation," 3rd Generation Partnership Project (3GPP), Technical Specification (TS) 38.211, Apr. 2025, release 18, version 18.6.0.
- [22] F. Liu *et al.*, "CP-OFDM achieves the lowest average ranging sidelobe under QAM/PSK constellations," *IEEE Trans. Inf. Theory*, vol. 71, no. 9, pp. 6950–6967, 2025.
- [23] Y. Zhang, S. Aditya, and B. Clerckx, "Input distribution optimization in ofdm dual-function radar-communication systems," *IEEE Trans. Signal Processing*, vol. 72, pp. 5258–5273, 2024.
- [24] M. F. Keskin *et al.*, "Fundamental trade-offs in monostatic ISAC: A holistic investigation towards 6G," *IEEE Trans. Wireless Commun.*, 2025.
- [25] Z. Du, F. Liu, Y. Xiong, T. X. Han, Y. C. Eldar, and S. Jin, "Reshaping the isac tradeoff under ofdm signaling: A probabilistic constellation shaping approach," *IEEE Trans. Signal Processing*, vol. 72, pp. 4782–4797, 2024.
- [26] F. Liu, Y. Xiong, S. Lu, S. Li, W. Yuan, C. Masouros, S. Jin, and G. Caire, "Uncovering the iceberg in the sea: Fundamentals of pulse shaping and modulation design for random isac signals," *IEEE Trans. Signal Processing*, vol. 73, pp. 2511–2526, 2025.
- [27] J. Hu *et al.*, "Learning-based constellation design for uplink bi-static integrated sensing and communication," *IEEE Trans. Veh. Technol.*, vol. 74, no. 8, pp. 13 219–13 224, 2025.
- [28] B. Geiger, F. Liu, S. Lu, A. Rode, and L. Schmalen, "Joint optimization of geometric and probabilistic constellation shaping for OFDM-ISAC systems," in *Proc. IEEE JC&S*, Jan. 2025.
- [29] Z. Du, F. Liu, Y. Xiong, T. X. Han, W. Yuan, Y. Cui, C. Yao, and Y. C. Eldar, "Probabilistic constellation shaping for OFDM-based ISAC signaling," in *2023 IEEE Globecom Workshops (GC Wkshps)*, Kuala Lumpur, Malaysia, 2023, pp. 509–514.
- [30] X. Yang *et al.*, "Constellation design for integrated sensing and communication with random waveforms," *IEEE Trans. Wireless Commun.*, vol. 23, no. 11, pp. 17 415–17 428, 2024.
- [31] R. D. Yates, "A framework for uplink power control in cellular radio systems," *IEEE J. Sel. Areas Commun.*, vol. 13, no. 7, pp. 1341–1347, 2002.
- [32] C. J. Leuschen and R. G. Plumb, "A matched-filter-based reverse-time migration algorithm for ground-penetrating radar data," *IEEE Transactions on geoscience and remote sensing*, vol. 39, no. 5, pp. 929–936, 2002.
- [33] P. Wojaczek, F. Colone, D. Cristallini, and P. Lombardo, "Reciprocal-filter-based STAP for passive radar on moving platforms," *IEEE Transactions on Aerospace and Electronic Systems*, vol. 55, no. 2, pp. 967–988, 2019.
- [34] K. Han, K. Meng, and C. Masouros, "Sensing-secure ISAC: Ambiguity function engineering for impairing unauthorized sensing," *IEEE Transactions on Wireless Communications*, vol. 25, pp. 5386–5400, 2026.
- [35] A. Papoulis and S. U. Pillai, *Probability, Random Variables, and Stochastic Processes*, 4th ed. New York: McGraw-Hill, 2002.
- [36] A. Goldsmith, *Wireless communications*. Cambridge university press, 2005.
- [37] T. K. Sarkar and O. Pereira, "Using the matrix pencil method to estimate the parameters of a sum of complex exponentials," *IEEE Antennas and propagation Magazine*, vol. 37, no. 1, pp. 48–55, 1995.

- [38] S. P. Boyd and L. Vandenberghe, *Convex optimization*. Cambridge university press, 2004.